SOLAR WIND-DRIVEN ELECTRON RADIATION BELT RESPONSE FUNCTIONS AT 100-MIN TIME SCALES

E.J. Rigler[1], D.N. Baker[1], R.S. Weigel[1], and D. Vassiliadis[2]

[1]*LASP, University of Colorado, 1234 Innovation Drive, Boulder, CO 80303, USA*
[2]*USRA at NASA Goddard Space Flight Center, code 692, Greenbelt, MD 20771, USA*

ABSTRACT

We present a simple yet numerically robust technique, using autoregressive linear filters, to remove unwanted "colored noise" from solar wind and radiation belt electron data at sub-daily resolution. The remaining signal is then studied using finite impulse response linear prediction filters to represent the driven portion of the linear dynamics that describe the coupling between solar wind speed and electron flux. Sub-daily resolution response profiles covering magnetic L-shells between 1.1 and 8.0 R_E are presented which are consistent with daily resolution response functions (Vassiliadis et al., 2002). Namely, while there is strong global coherence governing electron flux dynamics, there are at least two distinct responses. The first response is an immediate dropout of electrons between L=4 and L=7 that is at least a partly adiabatic effect associated with enhancements in the ring current. This is followed by a 1-2 day delayed enhancement across the same L-shells that is likely a result of increased radial diffusion. The second response is an immediate enhancement seen between L=3 and L=4 with a typical duration of less than one day. Plausible explanations for this second response are briefly discussed, but neither empirical nor theoretical evidence can establish conclusively a definite physical cause. Finally, the response profiles show significant solar cycle and seasonal dependencies, indicating that better model output might be achieved with: 1) additional simultaneous solar wind inputs; 2) more sophisticated dynamical model structures capable of incorporating non-linear feedback; and/or 3) time-adaptive linear filters that can track non-stationary dynamics in time.

INTRODUCTION

The tremendous quantity and high quality of solar, solar-wind, and magnetospheric data that has become available in recent years has led to a veritable renaissance in magnetospheric research. It has allowed for unprecedented testing, validation, and improvements in existing physics-based models, as well as a resurgence of interest in empirical and semi-empirical models for space weather specification and forecasting. Of particular practical and scientific interest is an improved description of the dynamics of trapped relativistic electrons. These "killer" electrons constitute one of the most technologically and economically damaging forms of space weather, due to their ability to induce both surface and deep dielectric charging and damage key satellite systems (Baker, 2002). This directly translates into a substantial risk to human welfare because of its dependence on satellites for communications, defense, remote sensing, and transportation.

While new data sets have helped advance our theoretical understanding of the physics responsible for the acceleration and loss of relativistic electrons in the magnetosphere, the resulting physics-based models are not particularly useful forecasting tools. This is primarily due to the overwhelming computational complexity required to model such a large range of time and spatial scales. Semi-empirical, or parameterized physical models are one approach for overcoming these computational limitations. Indeed, they have proved to be powerful predictors for certain regions of the radiation belts (e.g. Li et al., 2001). However, they are often biased in favor of a particular physical mechanism that may or may not dominate throughout the entire magnetosphere.

Many efforts have been made to develop more general dynamical models based on data alone. Early linear prediction filter studies focused primarily on the response of daily-averaged relativistic electrons at geostationary altitudes (e.g. Nagai, 1998; Baker et al., 1990). The technique proved to be a useful forecasting tool and has even been implemented in an operational environment at NOAA's Space Environment Center. More recently, Vassiliadis et al. (2002) extended this technique spatially by incorporating SAMPEX electron flux data into linear prediction filters for a broad range of L-shells from 1.1 to 10.0 R_E.

This paper presents a simple, yet numerically robust, method for improving linear prediction filters by increasing the time resolution at which the coupling of the solar wind to radiation belt electron fluxes can be modeled. This technique is then validated in a study of relativistic electron response functions across a broad region of trapped and quasi-trapped electrons in the Earth's magnetosphere, ultimately providing an improved description of the causative dynamics governing the acceleration and loss of these electrons at sub-daily time scales.

LINEAR PREDICTION FILTERS

A linear prediction filter is a simple dynamical model that consists of a vector of sequential linear coefficients that are convolved with an input time series in order to estimate a system's response to changes in that input series. These coefficients are determined using standard system identification techniques that minimize the difference between the filter output and actual observations (see Figure 1). Eq. (1) represents a single input, single output (SISO) finite impulse response (FIR) filter ("finite" because the response drops to zero when there is no further input).

$$\hat{y}_t = \sum_{j=p}^{n} f_j u_{t-j} \quad \text{or} \quad \begin{bmatrix} \hat{y}_0 \\ \hat{y}_1 \\ \vdots \\ \hat{y}_t \end{bmatrix} = \begin{bmatrix} u_{-p} & u_{-p-1} & \cdots & u_0 & \cdots & u_{-n-1} & u_{-n} \\ u_{-p+1} & u_{-p} & \cdots & u_1 & \cdots & u_{-n} & u_{-n+1} \\ \vdots & \vdots & & \vdots & & \vdots & \vdots \\ u_{-p+t} & u_{-p+t-1} & \cdots & u_t & \cdots & u_{-n+t-1} & u_{-n+t} \end{bmatrix} \cdot \begin{bmatrix} f_p \\ \vdots \\ f_0 \\ \vdots \\ f_n \end{bmatrix} \tag{1}$$

If FIR filter coefficients are determined via standard linear regression (the most common technique), they may be sub-optimal if autocorrelations exist in either the input and output time series. It is therefore desirable to remove, or otherwise account for, this "colored noise" in the training data.

Autoregressive (AR) linear prediction filters operate recursively by using previous system output as the current input, providing a kind of dynamic feedback, which allows them to reproduce recurrent signals. AR filters are typically designed as 1-step predictors, but are otherwise quite similar in form to FIR filters:

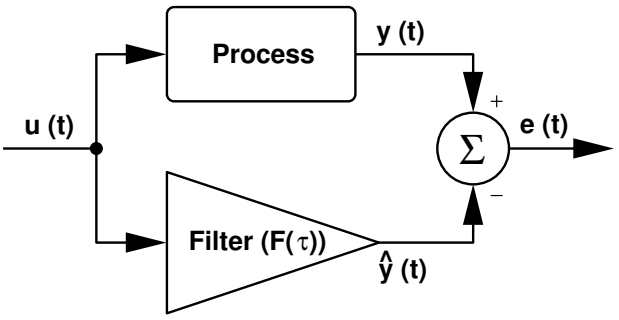

Fig. 1: General single input, single output (SISO) filter in a system identification configuration.

$$\hat{y}_t = \sum_{j=1}^{n} g_j y_{t-j} \quad \text{or} \quad \begin{bmatrix} \hat{y}_0 \\ \hat{y}_1 \\ \vdots \\ \hat{y}_t \end{bmatrix} = \begin{bmatrix} y_{-1} & y_{-2} & \cdots & y_{-n} \\ y_{-0} & y_{-1} & \cdots & y_{-n+1} \\ \vdots & \vdots & & \vdots \\ y_{t-1} & y_{t-2} & \cdots & y_{t-n} \end{bmatrix} \cdot \begin{bmatrix} g_1 \\ g_2 \\ \vdots \\ g_n \end{bmatrix} \tag{2}$$

A very general model structure can be formed by combining the FIR and AR filters, and solving for their respective coefficients simultaneously. This model structure possesses an external driver, but can still reproduce potentially infinite impulse response (IIR) functions, thus providing a simple yet robust mechanism for separating recurrent dynamics (diurnal variations and exponential decays often observed in radiation belt electron fluxes, for example) from responses driven directly by the input observations.

SOLAR WIND AND RADIATION BELT DATA

Relativistic Electrons - The Solar, Anomalous, and Magnetospheric Particle EXplorer (SAMPEX) satellite, launched in 1992, has a low-altitude (∼600 km), high-inclination (∼82°) orbit with a period of approximately 100 minutes (Baker et al., 1993). SAMPEX relativistic electron flux data from the ELO channel of the Proton Electron Telescope (Cook et al., 1993) is binned according to the International Geomagnetic Reference Field (IGRF). This results in four passes through each magnetic L-shell per orbit which are combined to provide orbit-averaged flux observations. Strong diurnal variations unrelated to geomagnetic local time often remain in the ELO orbit-averaged data, and are usually attributed to the rotation of geographically varying electron flux regions with respect to the relatively fixed orbit plane of the SAMPEX satellite. This is the "colored noise" that we wish to filter out so that the driven solar wind speed to radiation flux response can be better studied.

Solar Wind Speed - The solar wind data used in this study was taken from the OMNIWeb database, a compilation of hourly solar wind magnetic field and plasma measurements, taken from a variety of different satellites over the last several decades, and cross-normalized to provide multi-source uniformity (NSSDC, 2003). We limited our current study to include only solar wind bulk speed between 1994 and 1999, since the OMNI data density outside this range fell from an average of well over 80% to below 40%. Linear interpolation was used to fill data gaps, as well as to synchronize the hourly solar wind data with the 100-minute orbit-averaged SAMPEX data.

"Whitening" Training Data - A technique for separating recurrent from driven dynamics was described previously. This approach, however, only accounted for autocorrelations in the output data. Autocorrelations in the input data can also lead to sub-optimal filter coefficients. It is common practice to use a stand-alone AR model to pre-filter both the input and output data sets to remove any autocorrelations they have in common (Ljung, 1999). This process is referred to as "whitening" the data, and it was used to remove long-term recurrent signals in the training data associated with season and solar cycle.

SUB-DAILY RESPONSE FUNCTIONS AND L-SHELL PROFILES

Whitened solar wind speed and log-flux electron data were used to train the optimal coefficients for separate and independent IIR linear prediction filters for various L-shells. Figure 2 compares filter coefficients derived from daily-averaged solar wind and radiation belt observations (similar to Vassiliadis et al., 2002) with the filter coefficients calculated for the driven portion (i.e. f_j) of the orbit-averaged IIR filter for geostationary altitudes (i.e. L∼6.6).

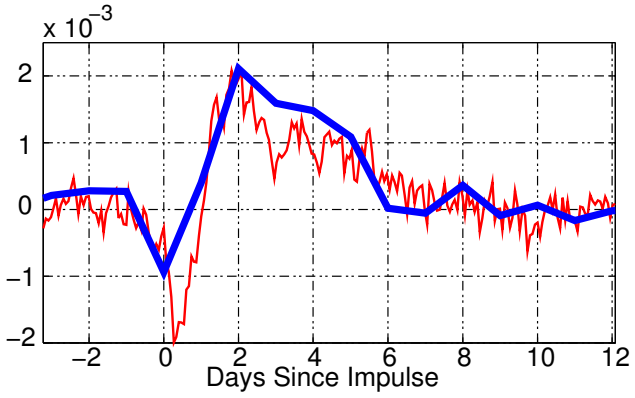

Fig. 2: Linear response functions of relativistic electrons at geostationary altitudes to unit-impulse changes in daily and ∼100 min. solar wind speed observations.

It should first be noted that the absolute scale of the orbit-averaged response function is somewhat arbitrary, since the true response requires both the FIR and AR portions of the filter to be considered. Next, it is clear that the dropout at zero-lag in the daily-average data response function is mostly causal (i.e. it occurs after solar wind impulses, and may be interpreted as a physical response) when examined at 100-minute time scales. This feature has been noted in prior studies (Baker et al., 1990) and can be at least partly attributed to adiabatic losses associated with changes in the ring current (often referred to as the D_{st} effect) (Kim et al., 1997; Li et al., 1997). Otherwise, it appears that there is little in the way of additional large-scale dynamical structure to be observed by using higher resolution data (the small-amplitude oscillations with frequencies at or above the Nyquist frequency, are most likely due to noisy data, although a more thorough analysis than we provide here is necessary to be certain).

The primary advantage afforded by using SAMPEX electron data is its spatial resolution and coverage. The driven response functions were calculated for electron flux from L=1.1 to L=8, with a resolution of 0.1 R_E. They were then ordered according to L-shell, and a 3×3 boxcar filter was used to smooth out some of the high-frequency noise (this corresponds to a ∼300 minute time, and 0.3 R_E spatial resolution). Finally, an 11-level contour plot was generated, centered at zero, and spaced every 5×10^{-4} flux units (no contour was drawn at zero so as to more clearly separate negative and positive responses).

The first panel in Figure 3 displays the response function profile for the entire training data set (1994-1999). The first notable feature in this profile is the immediate and short-lived negative response between L=4 and L=7, followed by a fairly extended positive response that peaks between one and two days after the solar wind impulse. This includes the response function obtained for geostationary altitudes, and is consistent with electron flux observations made during geomagnetic storms (e.g. Blake et al., 2001; Friedel et al., 2002). Moreover, this similarity in response functions throughout an extended portion of the magnetosphere supports the idea of strong and global dynamical coherence for relativistic electrons (Baker et al., 2001; Kanekal et al., 2001).

Perhaps the most surprising feature in this profile is the relatively strong, but short-lived, response between L=3 and L=4, immediately following changes in the solar wind speed. Baker et al. (1994) noted occasional, but strong enhancements in this region, and suggested that they were a result of extremely enhanced radial diffusion whose source population was comprised of electrons normally found around L=4-5. It also appears, however, to be strongly correlated with the negative response seen at higher L-shells, which leads one to believe it is at least partly adiabatic and related to changes in D_{st}. This concept was shown to be at least theoretically possible if electron phase-space density profiles did not increase smoothly with altitude (Kim et al., 2002).

The last three panels in Figure 3 show response function profiles for sequential two-year periods corresponding to: 1) the end of the declining phase of the solar cycle; 2) solar minimum; and 3) the beginning of the ascension to solar maximum. A solar cycle dependence is clear even with only six years worth of response function profiles. The years 1994 and 1995 were characterized by frequent high-speed solar wind streams and, perhaps correspondingly, extended periods of high electron fluxes in the radiation belts. The response function profile is somewhat noisier than the six-year average, and there is a weakly negative acausal (i.e. time-lags < 0) response between L=4 and L=6, indicating that the inclusion of additional solar wind inputs might improve predictions somewhat.

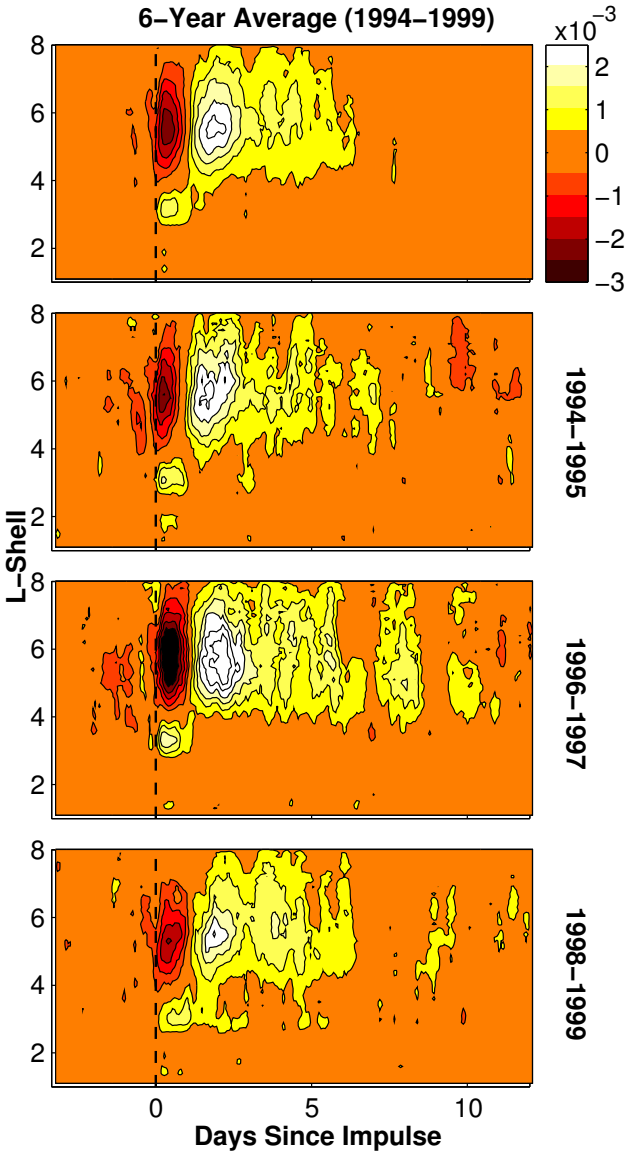

Fig. 3: The first panel is an L-shell profile of the 6-year averaged electron flux response to changing solar wind speed. The following three panels illustrate how this response changes as the solar cycle approaches its minimum (∼1996), and climbs back toward its maximum.

1996 and 1997 saw a significant decrease in both the average solar wind speed and its variability. There were strong but relatively short-lived electron flux enhancements, usually followed by significant periods of low fluxes (this low flux was especially pronounced near the middle of 1996). The response profile seems to represent both of these extremes, with strong negative responses immediately following solar wind events, and strong delayed enhancements. The immediate enhancement at lower L-shells is also stronger during this period. This is not proof of an adiabatic response, but it may indicate that the response is related to the negative response seen at higher L-shells.

Average solar wind speeds in 1998 and 1999 were higher than in 1996 or 1997, but not as high as 1994 or 1995. The relativistic electron fluxes were also significantly higher than in 1996 or 1997, at times reaching levels not seen since 1994. However, the response function profile clearly shows a weaker response. This would seem to indicate that, while the solar wind does indeed drive the enhancements seen in the radiation belt electrons, it does so in a

very non-linear manner. This is not surprising, perhaps, when it is noted that the increased solar wind speed was characterized by more short-lived, relatively impulsive events, rather than long-lived, high-speed streams. This may also be yet another indication that not all of the relevant inputs were considered in these linear coupling functions.

Figure 4 shows seasonally varying response profiles. Each response function is calculated by including the season's equinox/solstice, and the 90 days worth of data both preceding and following that date. This results in some overlap, but shorter time-spans did not provide enough quality data points to generate clean response functions. The final profile is therefore the average of each season for the 5 years fully encompassed by the training data.

The most prominent variation seen in these profiles is the weaker delayed enhancement seen between L=4 and L=7 in the summer. This is consistent with SAMPEX observations over the entire 1994-1999 period, with a particularly pronounced drop in electron fluxes in the summer of 1996. There is also a slight strengthening of the positive response between L=3 and L=4 during the winter. This is roughly consistent with SAMPEX observations, which show that deep "injections" of electrons tend to occur near the beginning/end of the years if they occur at all.

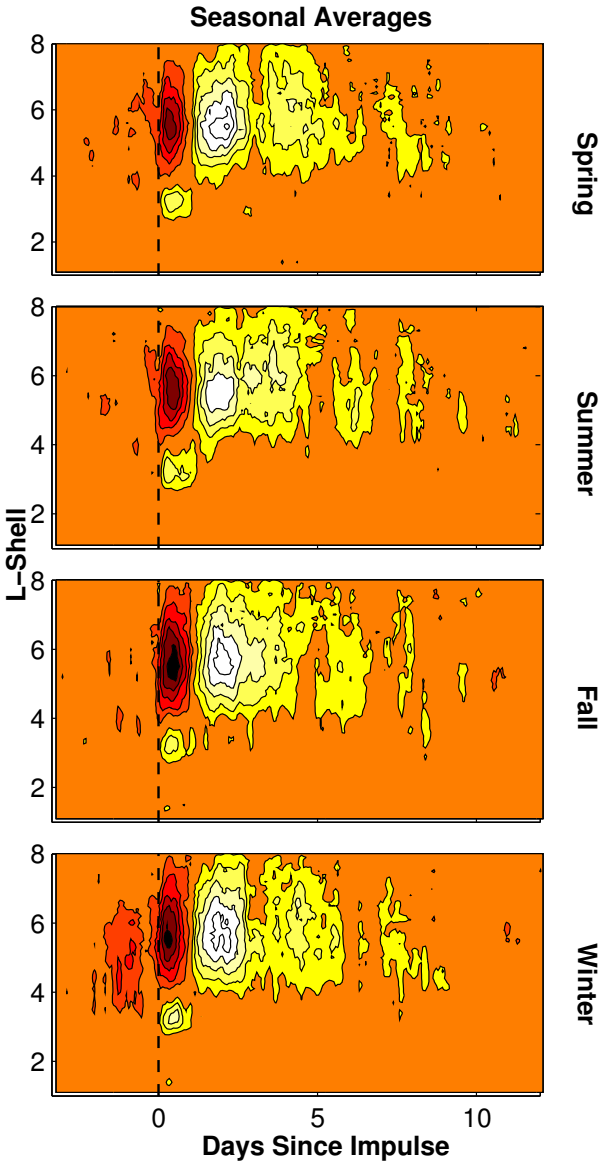

Fig. 4: These panels illustrate how the response of relativistic electrons to changing solar wind speed can vary with the northern hemisphere season.

SUMMARY AND CONCLUSIONS

We demonstrated a simple and robust numerical technique that uses autoregressive filters to remove unwanted "colored noise" from causally related time series in order to better study the driven linear response of radiation belt electrons to changing solar wind speed. The response functions were calculated for SAMPEX orbit-averaged data for each L-shell from 1.1 to 8.0, in bins of 0.1 R_E, and found to be mostly consistent with profiles generated by Vassiliadis et al. (2002) using daily-averaged solar wind and SAMPEX data. This included a demonstration of solar cycle and seasonal dependencies in the response profiles.

The non-stationarity of the dynamical relationship between the solar wind and the radiation belt electrons, in addition to non-zero acausal responses, is indicative of missing inputs, some sort of non-linear dynamical feedback that has not been considered in the simple linear model structure used in this study, or most likely some combination of both. The next logical step is to apply the techniques described in this paper to a variety of simultaneous solar wind measurements, and analyze the multi-channel electron response functions at sub-daily resolution. If the inclusion of additional inputs cannot fully account for the time-variance of the solar wind-radiation belt coupling, more sophisticated data-derived dynamical functions must be considered. These might incorporate non-linear feedback into either or both the driven and recurrent portions of the model, resulting in what is commonly referred to as a Box-Jenkins model (Box and Jenkins, 1976).

Finally, radiation belt dynamics are, in reality, simultaneously driven by a variety of inputs, whose relative coupling efficiencies all change with time. It is therefore unlikely that a completely time-invariant model can be derived with even the most sophisticated model structures. Time-adaptive filters will provide the most realistic description of the dominant dynamical mechanisms responsible for the tremendous variability seen in outer belt relativistic electrons, thereby providing an accurate and fully data-derived space weather specification and forecast tool.

ACKNOWLEDGMENTS

Thanks are extended to the SAMPEX data team and the NSSDC at Goddard Space Flight Center for providing the quality space physics data necessary to this research. This study was primarily supported by an NSF National Space Weather Program (NSWP) grant, award ATM-9819900.

REFERENCES

Baker, D.N., R.L. McPherron, T.E. Cayton, et al., Linear prediction filter analysis of relativistic electron properties at 6.6 RE, *J. Geophys. Res.*, **95**(A9), 15,133-15,140, 1990.

Baker, D.N., G.M. Mason, O. Figueroa, et al., An overview of the solar, anomalous, and magnetospheric particle explorer (SAMPEX) mission, *IEEE Trans. Geosci. Remote Sensing*, **31**(3), 531-541, 1993.

Baker, D.N., J.B. Blake, L.B. Callis, et al., Relativistic electron acceleration and decay times in the inner and outer radiation belts: SAMPEX, *Geophys. Res. Lett.*, **21**(6), 409-412, 1994.

Baker, D.N., S.G. Kanekal, J.B. Blake, et al., The global efficiency of relativistic electron production in the Earth's magnetosphere, *J. Geophys. Res.*, **106**(A9), 19,169-19178, 2001.

Baker, D.N., How to cope with space weather, *Science*, **297**, 1486-1487, 2002.

Blake, J.B. R.S. Selesnick, D.N. Baker, et al., Studies of relativistic electron injection events in 1997 and 1998, *J. Geophys. Res.*, **106**(A9), 19,157-19,168, 2001.

Box, G.E.P. and G.M. Jenkins, *Time Series Analysis: Forecasting and Control*, Holden-Day Inc., Oakland, CA, 1976.

Clauer, C.R., The technique of linear prediction filters applied to studies of solar wind-magnetosphere coupling, *Solar Wind-Magnetosphere Coupling*, pp. 39-57, Terra Scientific Pub. Co., Tokyo, 1986.

Cook, W.R., A.C. Cummings, J.R. Cummings, et al., A proton electron telescope for studies of magnetospheric, solar, and galactic particles, *IEEE Trans. Geosci. Remote Sensing*, **31**(3), 556-571, 1993.

Friedel, R.H.W., G.D. Reeves, and T. Obara, Relativistic electron dynamics in the inner magnetosphere – a review, *J. Atmos. Sol. Terr. Phys.*, **64**(2), 265-282, 2002.

Kanekal, S.G., D.N. Baker, and J.B. Blake, Multisatellite measurements of relativistic electrons: global coherence, *J. Geophys. Res.*, **106**(A12), 29,721-29,732, 2001.

Kim, H-J, A.A. Chan, Fully adiabatic changes in short time relativistic electron fluxes, *J. Geophys. Res.*, **102**(A10), 22,107-22,116, 1997.

Kim, H-J, G. Rostoker, and Y. Kamide, Radial dependence of relativistic electron fluxes for storm main phase development, *J. Geophys. Res.*, **107**(A11), doi:10.1029/ 2001JA007513, 2002.

Li, X., D.N. Baker, M. Temerin, et al., Multisatellite observations of the outer zone electron variation during the November 3-4, 1993, magnetic storm,, *J. Geophys. Res.*, **102**(A7), 14,123-14,140, 1997.

Li, X., M. Temerin, D.N. Baker, et al., Quantitative prediction of radiation belt electrons at geostationary orbit based on solar wind measurements, *Geophys. Res. Lett.*, **28**(9), 1887-1890, 2001a.

Li, X., D.N. Baker, S.G. Kanekal, et al., Long term measurements of radiation belts by SAMPEX and their variations, *Geophys. Res. Lett.*, **28**(20), 3827-3830, 2001b.

Ljung, L, *System Identification - Theory for the User, 2nd Ed.*, Prentice Hall PTR, Upper Saddle River, NJ, 1999.

Nagai, T., Space weather forecast: prediction of relativistic electron intensity at synchronous orbit, *Geophys. Res. Lett.*, **15**(5), 425-428, 1988.

Nelles, O., *Nonlinear System Identification: From Classical Approaches to Neural Networks and Fuzzy Models*, Springer-Verlag, Berlin Heidelberg, 2001.

NSSDC, *OMNIWeb - Near Earth Heliosphere Data*, National Space Science Data Center, NASA, `http://nssdc.gsfc.nasa.gov/omniweb/`, 2003.

Vassiliadis, D., A.J. Klimas, A. Valdivia, et al., The nonlinear dynamics of space weather, *Adv. Space Res.*, **26**(1), 197-207, 2000.

Vassiliadis et al., Long-term-average, solar cycle, and seasonal response of magnetospheric energetic electrons to the solar wind speed, *J. Geophys. Res.*, **107**(A11), doi:10.1029/ 2001JA000506, 2002.

E-mail address of E.J. Rigler: Jrigler@Colorado.EDU

Manuscript received 19 October 2002; revised 23 September 2003; accepted 23 September 2003